ANNALS OF GEOPHYSICS, VOL. 48, N. 4/5, August/October 2005

Geochemical modeling of magmatic gas scrubbing

Luigi Marini and Barbara Gambardella
Laboratorio di Geochimica, Dipartimento per lo Studio del Territorio e delle sue Risorse (DipTeRis), Università degli Studi di Genova, Italy

Abstract
The EQ3/6 software package, version 7.2 was successfully used to model scrubbing of magmatic gas by pure water at 0.1 MPa, in the liquid and liquid-plus-gas regions. Some post-calculations were necessary to account for gas separation effects. In these post-calculations, redox potential was considered to be fixed by precipitation of crystalline α-sulfur, a ubiquitous and precocious process. As geochemical modeling is constrained by conservation of enthalpy upon water-gas mixing, the enthalpies of the gas species of interest were reviewed, adopting as reference state the liquid phase at the triple point. Our results confirm that significant emissions of highly acidic gas species ($SO_{2(g)}$, $HCl_{(g)}$, and $HF_{(g)}$) are prevented by scrubbing, until dry conditions are established, at least locally. Nevertheless important outgassing of $HCl_{(g)}$ can take place from acid, HCl-rich brines. Moreover, these findings support the rule of thumb which is generally used to distinguish SO_2-, HCl-, and HF-bearing magmatic gases from SO_2-, HCl-, and HF-free hydrothermal gases.

Key words *magmatic gas – magma degassing – hydrothermal system – crater lake – meteoric water – scrubbing – reaction path modeling*

1. Introduction

Gases are released from magmas both during eruptions (syn-eruptive or active degassing) and in quiescent periods that either may preceed an eruption (pre-eruptive degassing) or may not (passive degassing). Studies of pre-eruptive degassing are of uppermost interest since we hope that we are able to interpret the changes in the composition and/or fluxes of volatiles as signals of the evolution of the magmatic system towards an eruptive episode. However, this is not a simple exercise due to the common occurrence of interfering processes, mainly magmatic gas scrubbing by waters and interaction of these aqueous solutions with rocks. The effects of water-rock interaction are enhanced by the high reactivity of most magmatic gases and are similar to what takes place in a Giggenbach's flask during fumarolic gas sampling. In particular, $CO_{2(g)}$, $H_2S_{(g)}$, $HCl_{(g)}$, and $HF_{(g)}$ are readily neutralised

$$CO_{2(g)} + OH^-_{(aq)} = HCO^-_{3(aq)} \quad (1.1)$$

$$H_2S_{(g)} + OH^-_{(aq)} = HS^-_{(aq)} + H_2O_{(l)} \quad (1.2)$$

$$HCl_{(g)} + OH^-_{(aq)} = Cl^-_{(aq)} + H_2O_{(l)} \quad (1.3)$$

$$HF_{(g)} + OH^-_{(aq)} = F^-_{(aq)} + H_2O_{(l)} \quad (1.4)$$

whereas the behavior of SO_2 is unique, in that it may be disproportionate to SO_4^{2-} and HS^-, as indicated by the reaction

$$4SO_{2(g)} + 7OH^-_{(aq)} = 3SO^{2-}_{4(aq)} + HS^-_{(aq)} + 3H_2O_{(l)} \quad (1.5)$$

Mailing address: Prof. Luigi Marini, Laboratorio di Geochimica, Dipartimento per lo Studio del Territorio e delle sue Risorse (DipTeRis), Università degli Studi di Genova, Corso Europa 26, 16132 Genova, Italy; e-mail: lmarini@dipteris.unige.it

but it can also produce many other aqueous S-bearing species and elemental sulfur (*e.g.*, Giggenbach, 1987, 1997).

In natural settings, scrubbing of magmatic gases is carried out by 1) the liquids hosted in the hydrothermal systems frequently interposed between the magma batch stationing at depth and the surface (*e.g.*, Reed, 1997; Symonds *et al.*, 2001; Marini *et al.*, 2003a); 2) the lacustrine waters stored in crater lakes (*e.g.*, Rowe *et al.*, 1992; Delmelle and Bernard, 2000; Varekamp *et al.*, 2001; Marini *et al.*, 2003b), and 3) the shallow meteoric waters soaking the volcanic edifice (*e.g.*, Symonds *et al.*, 2001). Interaction of magmatic gases with seawater can also occur, as possibly in the recent crisis of Panarea, Aeolian Islands, Italy (Chiodini *et al.*, 2002).

All these processes can be satisfactorily modeled by means of reaction path modeling, a powerful geochemical tool originally proposed by Helgeson (1968), who worked out the thermodynamic relationships needed to evaluate the irreversible gas-water-rock exchanges. The first computer code for reaction path modeling, PATHI, was developed by Helgeson and coworkers, who presented several applications, including hydrothermal rock alteration and ore deposition, in a series of ground breaking scientific papers (*e.g.*, Helgeson *et al.*, 1969).

The theoretical evolution of water composition and the changes in secondary mineral assemblages during progressive neutralization of an initially acidic aqueous solution originated by absorption of magmatic gases in meteoric water was modeled by Reed (1997), who recognised the appearance/disappearance of a series of intermediate *pH* buffers until the final, thermodynamically stable mineral paragenesis attains equilibrium with the aqueous solution. Although this theoretical model is in line with our present understanding of most hydrothermal systems with close magmatic association (Giggenbach, 1997), it cannot be applied throughout. For instance, this model fails to explain the origin of the deep, acidic Na-Cl-SO_4 waters of the Miravalles geothermal system (Costa Rica), which are probably generated through interaction of deep, neutral Na-Cl waters with rocks depleted in alkali and alkali-earth metals and enriched in SiO_2, Al_2O_3, and sulfate minerals, representing old solfataras buried by recent volcanics, as suggested by Bob Fournier in an informal communication about 10 years ago. Reaction path modeling supports the Fournier's hypothesis (Marini *et al.*, 2003a).

Gas-water-rock interactions in crater lake waters were modeled by Marini *et al.* (2003b) to investigate the reasons for the bimodal *pH* distribution in crater lake waters, which exhibit an acidic mode at *pH* 0.5-1.5 and a near neutral mode at *pH* 6-6.5 (Varekamp *et al.*, 2000). The neutralization of acid SO_4-Cl waters with andesite at both low temperature and high temperature, followed by cooling below 100°C, rarely produce aqueous solutions with *pH* in the 3.5-5 range, in line with available analytical data.

Reaction path modeling has recently been used to model magmatic gas scrubbing taking place through mixing of magmatic gas with air-saturated water, reaction of a magmatic gas/air-saturated water mixture with rock, and other processes in an excellent paper by Symonds *et al.* (2001). It turns out that scrubbing by water prevents significant $SO_{2(g)}$ and most $HCl_{(g)}$ emissions until dry pathways are established, apart from moderate $HCl_{(g)}$ degassing from acidic hydrothermal waters ($pH<0.5$). Degassing of $SO_{2(g)}$ from long-resident boiling hydrothermal systems is also prevented by magmatic gas scrubbing.

This paper investigates the irreversible gas-water mass exchanges taking place during addition of magmatic gas to pure water at 0.1 MPa, chiefly by means of the EQ3/6 software package, version 7.2 (Wolery, 1992; Wolery and Daveler, 1992). The purpose of this exercise is to test the EQ3/6 software package on a rather complex problem, which is similar to case 1 of Symonds *et al.* (2001). They modeled the addition of magmatic gas to air-saturated water instead of pure water as we intend to do. Hence, our results are not fully comparable with those of Symonds *et al.* (2001), as we neglect dissolved atmospheric gases (*i.e.*, $O_{2(aq)}$ and $N_{2(aq)}$) and, consequently, the derived N species (mainly $NH_4^+{}_{(aq)}$) in our computations. It must be stressed that the relatively high concentrations of $NH_4^+{}_{(aq)}$ predicted by Symonds *et al.* (2001) are based on the assumption of instantaneous

equilibration, which is rarely attained between N species in abiotic systems. On the other hand, the absence of dissolved O_2 in our model determines more reducing conditions, with respect to the model of Symonds *et al*. (2001), in the initial steps of gas-water interactions (ξ<0.4 mol) and, consequently, some differences in the concentrations of S species.

2. Setting up the model

The model consists in the progressive addition of hot magmatic gas into 1000 g of pure water initially at 25°C. Pressure is maintained at 0.1 MPa throughout the process. The magmatic gas is represented by sample 79-2 from Merapi Volcano, Indonesia (Le Guern *et al*., 1982), with a discharge temperature of 810°C and an equilibrium temperature of 915°C (Symonds *et al*., 1994). This is the same magmatic gas considered by Symonds *et al*. (2001) and its chemical composition is given in table I.

The overall process under investigation determines first the gradual heating of the aqueous solution from 25° to 100°C, second its gradual isothermal evaporation at 100°C, and third gas-gas mixing at increasing temperature. The first and second stages of the process, taking place in the pure liquid and liquid-plus-gas regions, can be modeled by means of the EQ3/6 software package, provided that some suitable pre-computations and post-calculations are carried out (see below). Upon total evaporation of the aqueous solution, the subsequent mixing of the gas phase thus produced with magmatic gas cannot be modeled by means of EQ3/6. However, simple mass-balance and equilibrium computations are sufficient to describe this gas-gas mixing process if the number of species considered is reasonably low.

Reaction path modeling in the pure liquid and liquid-plus-gas regions was performed in reaction path mode, through a purely stoichiometric approach, assuming immediate attainment of chemical equilibrium. The thermodynamic database COM was used. This is the most complete database available in the EQ3/6 software package and includes the thermodynamic properties of several solids, aqueous species, and gases, mostly derived from SUPCRT92 (Johnson *et al*., 1992).

In EQ3/6 runs, activity coefficients of ionic solutes were computed by means of the *B*-dot equation of Helgeson (1969).

Table I. Chemical composition (molar fractions) of the magmatic gas and of the gas produced through total vaporization of the liquid phase. Sample 79-2 from Merapi Volcano, Indonesia (Le Guern *et al*., 1982) is considered to be representative of the magmatic gas by Symonds *et al*. (2001) and in this study as well.

Gas species	Magmatic gas	Gas produced through total vaporization of the liquid
H_2O	0.8887	0.8532
CO_2	0.0707	0.09026
H_2	0.0154	1.49E-08
SO_2	0.0115	4.60E-06
H_2S	0.0112	0.00325
HCl	0.0059	0.0528
CO	0.0016	4.90E-13
S_2	0.0008	8.81E-10
HF	0.0004	0.00055
Discharge temperature	810°C	-
Equilibrium temperature	915°C	100°C
Molecular weight	20.59	21.39

2.1. *The enthalpy of liquid water and gas species*

Modeling is also based on the assumption of conservation of enthalpy upon water-gas mixing. The enthalpies tabulated in SUPCRT92 are apparent standard molal enthalpies of formation from the elements, as defined by Benson (1968), and cannot be used for these computations. In steam tables a different reference state is chosen, either liquid water at 0°C (Denbigh, 1971) or liquid water at the triple point, *i.e.*, 273.16 K, 0.006113 MPa. The latter reference state, with $S_{H_2O_{(l),\,triple}}=0$, $G_{H_2O_{(l),\,triple}}=0$, was adopted by the 5th International Conference on the Properties of Steam (Helgeson and Kirkham, 1974). For our purpose, the same convention must be adopted not only for H_2O, but also for all the gas species of interest. Therefore, for all gas species, we obtained the enthalpy value at the triple point consistent with this convention (see table II for details). The enthalpy of the *i*-th gas species at any temperature T and any pressure P (0.1 MPa in our case) can be computed by means of the relation (*e.g.*, Denbigh, 1971)

Table II. Triple point temperature, enthalpy at the triple point, and coefficients of the empirical power series in the temperature, which were used in this work to fit the molar heat capacity of relevant gas species and liquid water (C_P data from Chase, 1998).

Species	T_{triple} K	H_{triple} Jmol^{-1}	a Jmol^{-1}K^{-1}	b Jmol^{-1}K^{-2}	c Jmol^{-1}K^{-3}	d Jmol^{-1}K^{-4}	e Jmol^{-1}K^{-5}	f Jmol^{-1}K^{-6}	g Jmol^{-1}K^{-7}
$H_2O_{(l)}$	273.16 ([a])	0.00 ([a])	170.293	−9.821E-01	3.833E-03	−6.808E-06	4.755E-09		
$H_2O_{(g)}$	273.16 ([a])	45063 ([a])	33.791	−7.490E-03	2.777E-05	−1.582E-08	3.049E-12		
$H_{2(g)}$	13.95 ([b])	831.8 ([b])	14.668	1.127E-01	−3.400E-04	5.106E-07	−4.052E-10	1.639E-13	−2.665E-17
$CH_{4(g)}$	90.69 ([c])	7555 ([b])	35.277	−4.261E-02	1.946E-04	−1.535E-07	3.854E-11		
$CO_{(g)}$	68.13 ([c])	5684 ([b])	29.803	−8.247E-03	2.382E-05	−1.547E-08	3.243E-12		
$CO_{2(g)}$	216.58 ([c])	19346 ([b])	23.068	5.714E-02	−3.260E-05	6.791E-09			
$S_{2(g)}$	387.15 ([d])	34100 ([f])	26.747	2.493E-02	−2.029E-05	6.008E-09			
$H_2S_{(g)}$	187.6 ([c])	16500 ([f])	33.765	−1.031E-02	4.991E-05	−3.573E-08	8.182E-12		
$SO_{2(g)}$	197.64 ([b])	17400 ([f])	28.044	4.950E-02	−2.869E-05	5.705E-09			
$HCl_{(g)}$	159.0 ([c])	14000 ([f])	28.953	2.914E-03	−1.563E-05	3.215E-08	−2.162E-11	4.849E-15	
$HF_{(g)}$	151 ([e])	13300 ([f])	29.059	1.046E-03	−4.412E-06	6.534E-09	−2.073E-12		
$N_{2(g)}$	63.14 ([b])	2011 ([b])	28.757	6.667E-03	−4.163E-05	1.066E-07	−1.103E-10	5.186E-14	−9.259E-18
$NH_{3(g)}$	195.4 ([c])	25055 ([b])	33.142	−9.534E-03	8.160E-05	−6.472E-08	1.627E-11		

([a]) After Keenan *et al*. (1978): the reported H_{triple} value of 0.01 J/g for liquid water was set to 0 and the H_{triple} value of steam (2501.3 J/g) was changed accordingly.
([b]) NIST Chemistry WebBook (http://webbook.nist.gov/).
([c]) Lide (2002).
([d]) Castellan (1971).
([e]) Extrapolated value based on T_{triple} of HCl, HBr, and HI (from reference ([c])) and atomic number of halogens.
([f]) Value computed by means of the equation $\Delta H_{vap}=21\times4.184\times T_{vap}$, which is based on the Trouton's rule; this can be applied to non-associated liquids at $T_{vap}>150$ K (*e.g.*, Castellan, 1971).

$$H_T = H_{\text{triple}} + \int_{T\ \text{triple}}^{T} C_P\,dT + \int_{P\ \text{triple}}^{P} V(1-\alpha T)\,dP \tag{2.1}$$

where C_P is the molar heat capacity, V is the molar volume, and α is the coefficient of thermal expansion of the i-th gas species. As usually done in the literature (*e.g.*, Denbigh, 1971, and references therein), the heat capacity of gas species was expressed as empirical power series in the temperature (table II)

$$C_P = a + bT + cT^2 + dT^3 + \ldots \tag{2.2}$$

fitting the C_P data reported by Chase (1998). Consequently, the first integral of eq. (2.1) was computed as follows:

$$\int_{T\ \text{triple}}^{T} C_P\,dT = a(T - T_{\text{triple}}) + \frac{b}{2}(T^2 - T_{\text{triple}}^2) + \\ + \frac{c}{3}(T^3 - T_{\text{triple}}^3) + \frac{d}{4}(T^4 - T_{\text{triple}}^4) + \ldots \tag{2.3}$$

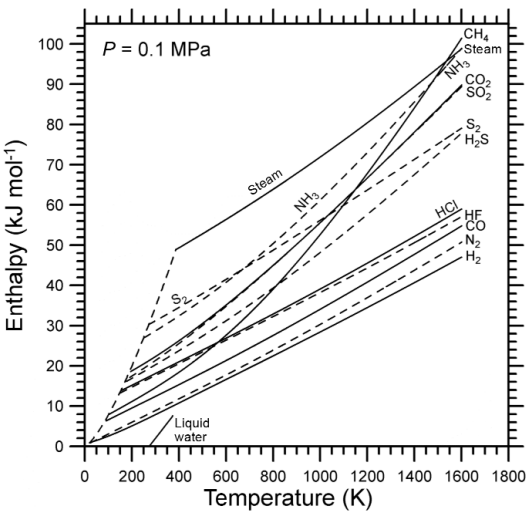

Fig. 1. Enthalpies of $H_2O_{(l)}$, $H_2O_{(g)}$, $H_{2(g)}$, $CO_{2(g)}$, $CO_{(g)}$, $CH_{4(g)}$, $N_{2(g)}$, $NH_{3(g)}$, $S_{2(g)}$, $SO_{2(g)}$, $H_2S_{(g)}$, $HCl_{(g)}$, and $HF_{(g)}$ at 0.1 MPa pressure and variable temperature.

whereas the second integral of eq. (2.1) was neglected assuming ideal gas behavior. In fact, for ideal gases $V=RT/P$, and

$$\alpha \equiv \frac{1}{V}\left(\frac{\partial V}{\partial T}\right)_P = \frac{R}{VP} = \frac{1}{T}. \tag{2.4}$$

It follows that:

$$1-\alpha T=0 \quad \text{and} \quad \int_{P\ triple}^{P} V(1-\alpha T)\,dP = 0\,.$$

This assumption is reasonable in the case under consideration, due to the comparatively small pressure increments from P_{triple} to 0.1 MPa pressure.

Computed enthalpies for $H_2O_{(l)}$, $H_2O_{(g)}$, $H_{2(g)}$, $CO_{2(g)}$, $CO_{(g)}$, $CH_{4(g)}$, $N_{2(g)}$, and $NH_{3(g)}$ are in excellent agreement with those reported by the NIST Chemistry WebBook (http://webbook.nist.gov/). Enthalpies of $H_2O_{(l)}$, $H_2O_{(g)}$, $H_{2(g)}$, $CO_{2(g)}$, $CO_{(g)}$, $CH_{4(g)}$, $N_{2(g)}$, $NH_{3(g)}$, $S_{2(g)}$, $SO_{2(g)}$, $H_2S_{(g)}$, $HCl_{(g)}$, and $HF_{(g)}$ at 0.1 MPa pressure and variable temperature are shown in fig. 1. This plot shows that, at magmatic temperatures (let us say >800 K): a) the enthalpy of any gas is significantly higher than that of liquid water; and b) $H_2O_{(g)}$ has the highest enthalpy and is generally followed by $CH_{4(g)}$, $NH_{3(g)}$, $CO_{2(g)}$, $SO_{2(g)}$, $S_{2(g)}$, and $H_2S_{(g)}$, whereas $HCl_{(g)}$, $HF_{(g)}$, $CO_{(g)}$, $N_{2(g)}$, and $H_{2(g)}$ have much lower enthalpy values. From a) it follows that the temperature of liquid water is expected to increase upon input of magmatic gases of any composition. However, considering that the main constituent of magmatic gases is by far $H_2O_{(g)}$, followed by $CO_{2(g)}$ and $SO_{2(g)}$ (*e.g.*, Symonds *et al.*, 1994), the enthalpy of magmatic gases is not expected to diverge substantially from that of pure steam.

2.2. *Isobaric heating of the aqueous solution from 25° to 100°C*

Conservation of enthalpy upon water-gas mixing is conveniently expressed by the following equation:

$$H_{m,Tm} = H_{w,Tw}\,\frac{1000}{MW_w} + n_g \sum_j H_{j,Tg} X_j \tag{2.5}$$

where indices w, g, and m indicate the initial pure water, the magmatic gas, and the aqueous solution formed upon addition of n_g moles of magmatic gas to 1000 g of pure water, MW_w is the molecular weight of water, and X_j is the molar fraction of the j-th gas species in the magmatic gas. Both the enthalpies of solute species and the enthalpy of mixing are neglected. The temperature of the aqueous solution was derived from the enthalpy computed by eq. (2.5), based on the first relationship in table II solved with respect to T, *i.e.*

$$T(°C) = -0.07 + 13.282 H_{m,Tm} - .0033401 H_{m,Tm}^2. \quad (2.6)$$

Then, temperature was related to the reaction progress variable ξ, *i.e.*, the moles of magmatic gas added to 1000 g of pure water, by means of a second-degree polynomial equation. This is

$$T(°C) = 25.0 + 18.696\xi - 0.28003\xi^2 \quad (2.7)$$

for the considered example and was used to constrain reaction path modeling by EQ6 in the temperature range 25-99°C.

It must be noted that, in the system under consideration, the aqueous solution attains saturation with respect to crystalline α-sulfur upon addition of 0.022 mol of magmatic gas. This fact has to be taken into account in post-calculations (see below).

For ξ<0.4 mol, the total fluid pressure, obtained by summing the partial pressures of gas species (mainly H_2O, CO_2, and H_2S) given by EQ6, is lower than the external pressure of 0.1 MPa and results of EQ6 are fully representative. For $\xi \geq 0.4$ mol, total fluid pressure exceeds 0.1 MPa, indicating that the aqueous solution experiences gas exsolution (degassing) until total fluid pressure attains 0.1 MPa. Single-step degassing was modeled starting from the compositions of the aqueous phase computed by EQ6, referring to the following mass balance:

$$\left(\frac{n_j}{n_{H_2O}}\right)_o = \left(\frac{n_j}{n_{H_2O}}\right)_g f + \left(\frac{n_j}{n_{H_2O}}\right)_l (1-f) \quad (2.8)$$

and assuming equilibrium gas-liquid partitioning of gas species, *i.e.*

$$B_j = \frac{\left(\frac{n_j}{n_{H_2O}}\right)_g}{\left(\frac{n_j}{n_{H_2O}}\right)_l} \quad (2.9)$$

where the subscripts o, g, and l indicate the initial undegassed liquid, the separated gas and the degassed liquid phase, respectively, and f is the fraction of separated gas. Only $CO_{2(g)}$, $H_2S_{(g)}$, and $H_2O_{(g)}$ are present in significant contents in the separated gas phase. Water partial pressure was assumed to be fixed by temperature. The partition coefficients B_j of CO_2 and H_2S were computed from gas solubility data (Henry's constants) reported in the COM thermodynamic database of EQ3/6, $K_{H,j}$, and P_{H_2O}, by means of the equation

$$B_j = \frac{K_{H,j}}{P_{H_2O}}. \quad (2.10)$$

To compute degassing effects, f was tentatively varied until total fluid pressure equalled 0.1 MPa. At this point it was necessary to recompute the composition of the degassed liquid phase, a fact that is complicated by the change in redox conditions caused by H_2S loss. However, concurrent precipitation of crystalline α-sulfur (see above) constrains f_{O_2}, as expressed by the reaction

$$S_{(c)} + H_2O_{(l)} = 1/2 O_{2(g)} + H_2S_{(aq)}. \quad (2.11)$$

Oxygen fugacity was, therefore, computed based on the thermodynamic constant of reaction (2.11) and the activity of H_2S in the degassed liquid phase, which is assumed to be equal to its molality. This is a reasonable assumption for neutral aqueous species. The composition of the degassed liquid was then recomputed by means of EQ3NR, introducing temperature, f_{O_2}, f_{CO_2}, f_{H_2S}, and total Cl and F molalities, as input data, and forcing pH by the electroneutrality condition. The differences between the pH values thus computed and those of the initial undegassed liquid are in all cases except one less than 0.0004 pH units, probably due to rounding off effects. This virtual pH constancy upon gas loss is not surprising as the aqueous phase is a relatively dilute solution of strong acids (see below).

2.3. *Isobaric-isothermal evaporation at 100°C*

During this second stage of the overall process, temperature is kept constant at 100°C by $H_2O_{(l)}$-$H_2O_{(g)}$ coexistence. Initially, progressive addition of magmatic gas to water was modeled by means of EQ6 neglecting the effects of gas separation. Knowing the enthalpy of the aqueous solution (computed by eq. (2.5)), the fraction of separated steam, $y = n_{H_2O_{(g)}}/(n_{H_2O_{(g)}} + n_{H_2O_{(l)}})$, was then calculated assuming isoenthalpic boiling, *i.e.*

$$H_o = H_{H_2O_{(l)}} \cdot n_{H_2O_{(l)}} + H_{H_2O_{(g)}} \cdot n_{H_2O_{(g)}} + H_{CO_{2(g)}} \cdot n_{CO_{2(g)}} \tag{2.12}$$

and equilibrium gas-liquid partitioning of CO_2 (eq. (2.9)). Subscripts *o*, *l*, and g refer to the unboiled aqueous solution, the separated (boiled) liquid phase and the separated gas phase. Since H_2O and CO_2 represent more than 98% (on molar basis) of the gas species present in the separated gas phase, other gas species were neglected in eq. (2.12). Obtained *y* values were used to distribute the moles of each chemical species computed by EQ6 between the separated liquid and gas phases by means of simple mass balances (equivalent to eq. (2.8) with *y* instead of *f*), assuming equilibrium partitioning for gas species (eq. (2.9)). Again, partition coefficients were computed from the gas solubility data reported in the COM thermodynamic database of EQ3/6 by means of eq. (2.10) and f_{O_2} was calculated referring to reaction (2.11). Then the composition of the boiled liquid was recomputed by means of EQ3NR as for the first stage of the process. In this case, the differences between computed *pH* values and those of the unboiled aqueous solution range from 0.005 to 0.09 *pH* units, since the change in *pH* upon boiling cannot be properly accounted for by a simple mass balance like eq. (2.8).

2.4. *Isobaric gas-gas mixing at 100-915°C*

For this stage of the process, first we computed the specific enthalpy of the gas mixture H_{gm}, referring to water only, *i.e.*, by the equation

$$H_{gm} = \frac{H_{H_2O_{(g),T_S}} \cdot \left(\frac{1000}{MW_w} + n_{g,ev} \cdot X_{H_2O}\right) + H_{H_2O_{(g),T_g}} \cdot n_g \cdot X_{H_2O}}{\left(\frac{1000}{MW_w} + n_{g,ev} \cdot X_{H_2O}\right) + n_g \cdot X_{H_2O}} \tag{2.13}$$

in which subscript T_S is the saturation temperature (100°C) at the considered pressure (0.1 MPa), $n_{g,ev}$ indicates the moles of magmatic gas consumed to evaporate the aqueous solution completely, and n_g are the moles of magmatic gas added to the system after complete vaporization of the liquid. The first term of the numerator refers to the enthalpy of the steam produced through total vaporization of the aqueous solution and the first term of the denominator identifies the corresponding moles of steam. The second term of the numerator represents the enthalpy of the magmatic steam added to the system after complete vaporization of the liquid and the second term of the denominator identifies the corresponding moles of magmatic steam. The temperature of the gas mixture was derived from the enthalpy computed by eq. (2.13), based on the H_{H_2O}-*T* relationship (table II) solved with respect to *T*, *i.e.*

$$T(°C) = -1529.4 + 38.84 \cdot H_m - 0.1088 \cdot H_m^2 + 6.975 \cdot 10^{-5} \cdot H_m^3. \tag{2.14}$$

The molar fraction of magmatic steam in the gas mixture, x_s, was readily computed as follows:

$$x_s = \frac{n_g \cdot X_{H_2O}}{\left(\frac{1000}{MW_w} + n_{g,ev} \cdot X_{H_2O}\right) + n_g \cdot X_{H_2O}} \tag{2.15}$$

and used to calculate the concentrations of major gas species ($H_2O_{(g)}$, $CO_{2(g)}$, $SO_{2(g)}$, $H_2S_{(g)}$, $HCl_{(g)}$, and $HF_{(g)}$) in the gas mixture by means of simple mass balances, based on the compositions of the magmatic gas (table I) and of the gas produced through total vaporization of the aqueous solution. The concentrations of minor gas species ($H_{2(g)}$, $CO_{(g)}$, $S_{2(g)}$) in the gas mixture were then calculated referring to the following reactions:

$$H_2S_{(g)} + 2H_2O_{(g)} = SO_{2(g)} + 3H_{2(g)} \quad (2.16)$$

$$CO_{2(g)} + H_{2(g)} = H_2O_{(g)} + CO_{(g)} \quad (2.17)$$

$$H_2S_{(g)} = \frac{1}{2}S_{2(g)} + H_{2(g)} \quad (2.18)$$

whose thermodynamic constants were obtained by means of SUPCRT92 (Johnson *et al*., 1992).

3. Addition of magmatic gas to pure water at 0.1 MPa: modeling results

Apart from minor differences arising from the choice of modeling magmatic gas scrubbing by pure water rather than by air-saturated water, our results are very similar to those of Symonds *et al*. (2001).

3.1. *Temperature*

The plot of temperature *versus* the reaction progress variable ξ (fig. 2) shows a comparatively smooth increase from the initial temperature of liquid water, 25°C, to the saturation temperature at 0.1 MPa pressure (100°C). However, the transition from the single liquid phase region to the biphase liquid-plus-gas region occurs at ξ of 0.4 mol (see above), corresponding to a temperature of 32.4°C only. The temperature of 100°C is attained through addition of 4.29 mol of magmatic gas and it is kept constant up to ξ of 79.3 moles by coexistence of $H_2O_{(l)}$ and $H_2O_{(g)}$. Upon dry-up of the system, temperature immediately experiences a very sharp increase. Then it flattens for temperatures approaching that of the magmatic gas, 915°C.

3.2. *Redox potential*

The diagram of $\log f_{O_2}$ *versus* ξ (fig. 3a) is similar in shape to fig. 2, due to the marked temperature dependence of $\log f_{O_2}$. As shown by fig. 4a, $\log f_{O_2}$ values are initially intermediate between those fixed by the FeO-$FeO_{1.5}$ hydrothermal redox buffer (Giggenbach, 1987, temperature in Kelvin)

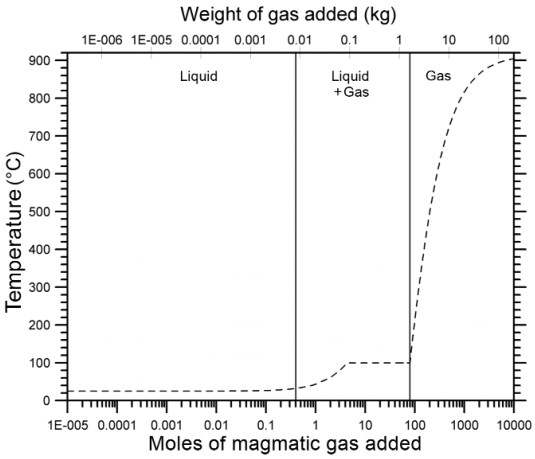

Fig. 2. Changes in temperature during the progressive addition of hot (915°C) magmatic gas into 1000 g of pure water initially at 25°C. Pressure was kept at 0.1 MPa throughout the simulation.

$$\log f_{O_2} = 10.736 - \frac{25414}{T} \quad (3.1)$$

and those constrained by the H_2S-SO_2 magmatic redox buffer (Giggenbach, 1987)

$$\log f_{O_2} = 2.657 - \frac{18251}{T} + \frac{2}{3}\log f_{H_2O}. \quad (3.2)$$

The latter buffer is closely approached upon dry-up of the system, when the $SO_{2(g)}$ concentration in the gas phase equals that of $H_2S_{(g)}$ (see below).

The evolution of the R_H parameter against ξ and temperature is shown in figs. 3b and 4b, respectively. This parameter is defined as $R_H = \log f_{H_2}/f_{H_2O} \cong \log X_{H_2}/X_{H_2O}$ (Giggenbach, 1987) and, therefore, it is directly comparable with the analytical data of fumaroles.

3.3. *Sulfur precipitation*

As anticipated, the aqueous solution becomes saturated with respect to crystalline α-sulfur upon addition of 0.022 mol of magmatic gas. In the log (moles of S) - logξ plot (fig. 5), the moles of S precipitated experience a very sharp initial in-

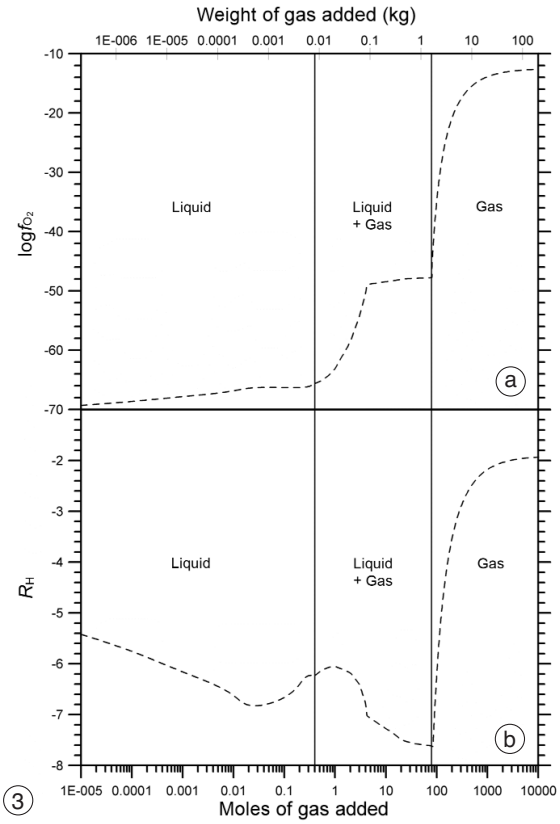

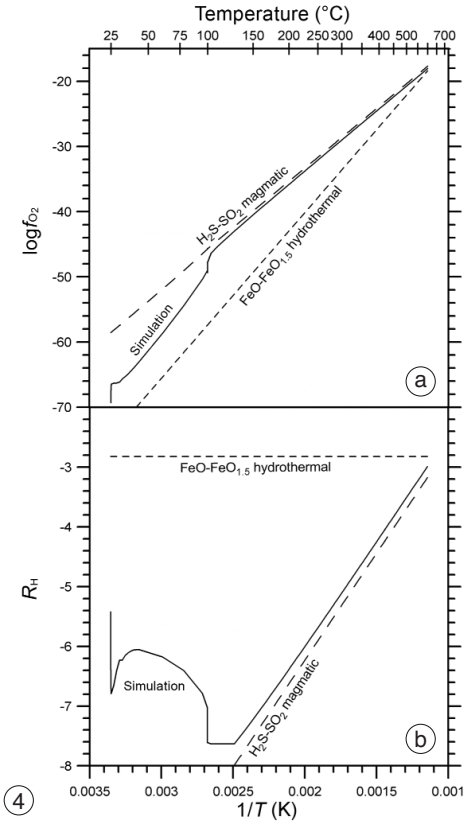

Fig. 3a,b. Variations in a) oxygen fugacity and b) $R_H = \log f_{H_2}/f_{H_2O} \cong \log X_{H_2}/X_{H_2O}$ during the progressive addition of hot (915°C) magmatic gas into 1000 g of pure water initially at 25°C. Pressure was kept at 0.1 MPa throughout the simulation.

Fig. 4a,b. Plot of a) $\log f_{O_2}$ and b) R_H *versus* temperature showing the expected changes in these variables during the progressive addition of hot (915°C) magmatic gas into 1000 g of pure water, initially at 25°C (line labelled simulation). Pressure was kept at 0.1 MPa throughout the simulation. Also shown are the FeO-$FeO_{1.5}$ hydrothermal redox buffer and the H_2S-SO_2, magmatic redox buffer of Giggenbach (1987). The latter was computed for the same f_{H_2O} of the computer simulation.

crease, but for ξ>0.14 they follow a linear trend which is parallel to that of the moles of S added to the system. This means that for ξ>0.14 mol the ratio between the amount of S removed from the system and the amount of S added to the system is constant. Since this ratio is 0.81, it can be concluded that most of the S added to the system is precipitated as crystalline α-sulfur, as already observed by Symonds *et al*. (2001).

3.4. *Chemistry of the liquid phase*

The *pH* of the aqueous solution decreases almost linearly with logξ, up to ξ of ~40 mol (fig. 6), whereas the decrease in *pH* becomes dramatic above this threshold, when the liquid phase is essentially a very concentrated aqueous solution of hydrogen chloride. In particular, the «last drop» of liquid (for ξ of 79.3 moles

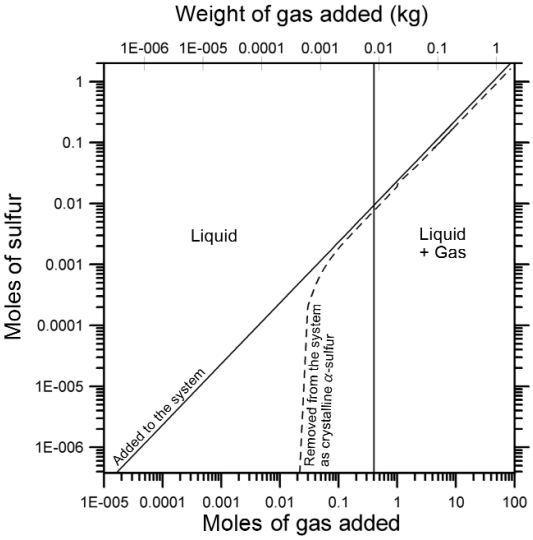

Fig. 5. Moles of sulfur both added to the system and precipitated as crystalline α-sulfur during the progressive addition of hot (915°C) magmatic gas into 1000 g of pure water initially at 25°C. Pressure was kept at 0.1 MPa throughout the simulation.

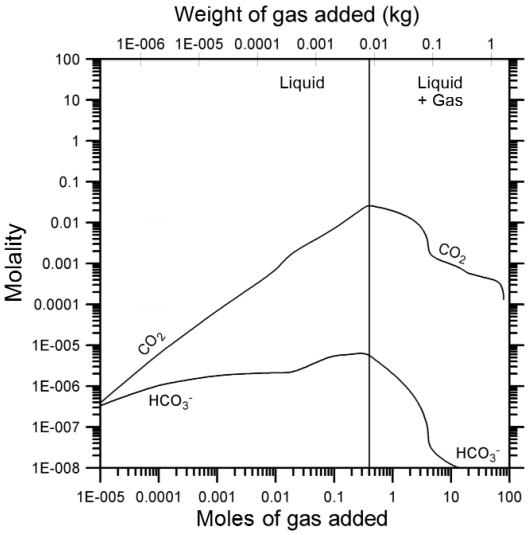

Fig. 7. Changes in dissolved carbonate species during the progressive addition of hot (915°C) magmatic gas into 1000 g of pure water initially at 25°C. Pressure was kept at 0.1 MPa throughout the simulation.

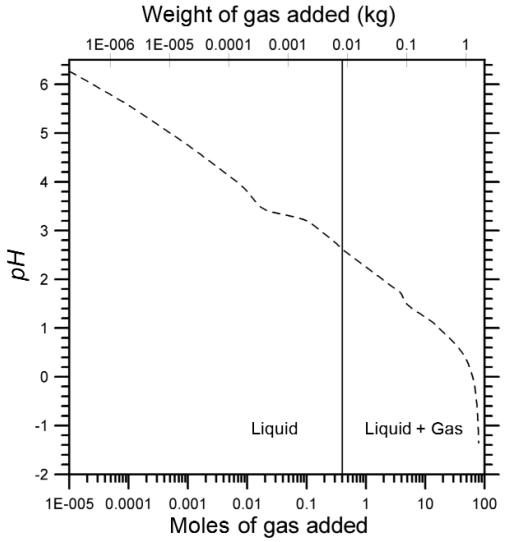

Fig. 6. Changes in the *pH* of the aqueous solution during the progressive addition of hot (915°C) magmatic gas into 1000 g of pure water initially at 25°C. Pressure was kept at 0.1 MPa throughout the simulation.

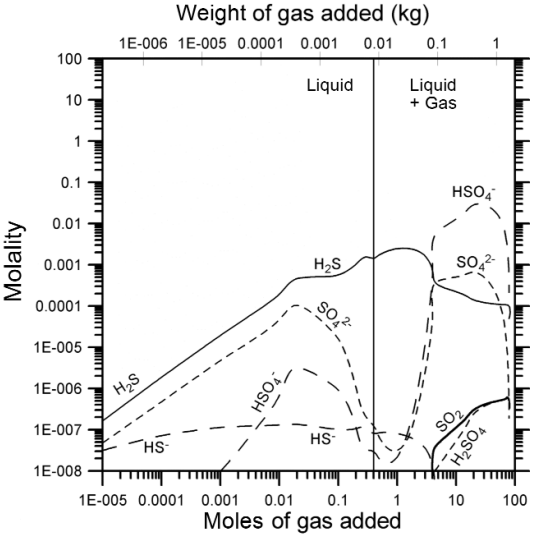

Fig. 8. Changes in dissolved sulfur species during the progressive addition of hot (915°C) magmatic gas into 1000 g of pure water initially at 25°C. Pressure was kept at 0.1 MPa throughout the simulation.

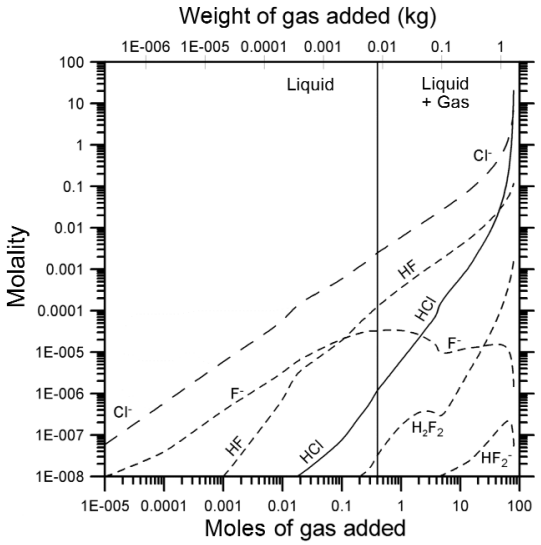

Fig. 9. Changes in dissolved chloride and fluoride species during the progressive addition of hot (915°C) magmatic gas into 1000 g of pure water initially at 25°C. Pressure was kept at 0.1 MPa throughout the simulation.

and y of 0.993) is dominated by $HCl_{(aq)}$, with a molality of 20.2, followed by H^+ and Cl^-, which are present with equal molalities of 7.96. Since activity coefficients of ionic solutes were computed by means of the *B*-dot equation of Helgeson (1969), which is expected to be accurate only in dilute aqueous solutions (*i.e.*, for ionic strength lower than 1 molal; Wolery, 1992), these values are highly uncertain.

On the one hand, the concentrations of dissolved CO_2 and H_2S (which enter preferentially the gas phase, with B_i at 100°C of 1405 and 29.8, respectively) increase with ξ in the single liquid phase but experience a marked decrease with ξ upon transition from the single liquid region to the biphase liquid-plus-gas region (figs. 7 and 8). The corresponding dissociation products, *i.e.*, HCO_3^- and HS^- ions, show variations similar to those of CO_2 and H_2S. On the other hand, the concentrations of dissolved HCl and HF (which preferentially remain into the liquid phase, with B_i at 100°C of 0.00121 and 0.00221, respectively) increase continuously with ξ, both in the liquid region and in the liquid-plus-gas region (fig.

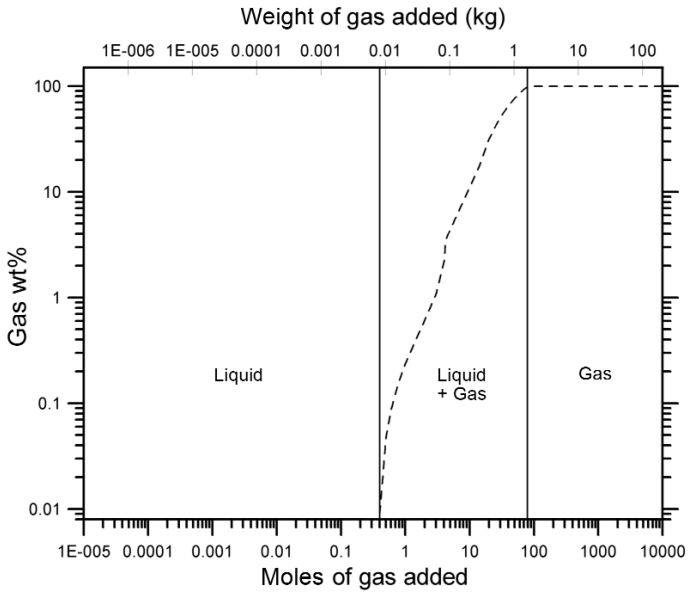

Fig. 10. Weight percentage of gas in the system during the progressive addition of hot (915°C) magmatic gas into 1000 g of pure water initially at 25°C. Pressure was kept at 0.1 MPa throughout the simulation.

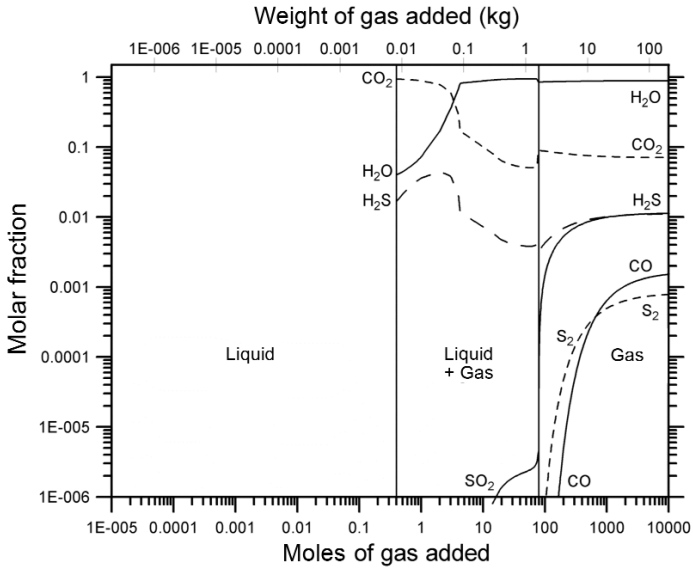

Fig. 11. Variations in the molar fractions of $H_2O_{(g)}$, $CO_{2(g)}$, $H_2S_{(g)}$, $SO_{2(g)}$, $CO_{(g)}$, and $S_{2(g)}$, during the progressive addition of hot (915°C) magmatic gas into 1000 g of pure water initially at 25°C. Pressure was kept at 0.1 MPa throughout the simulation.

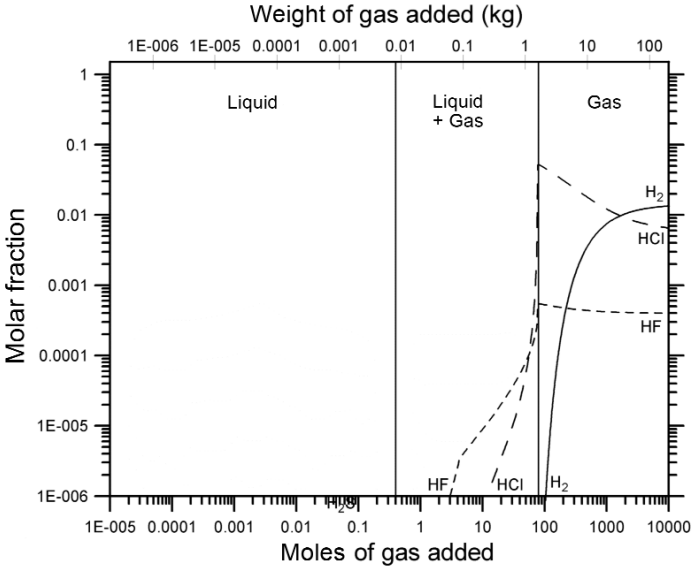

Fig. 12. Variations in the molar fractions of $H_{2(g)}$, $HCl_{(g)}$, and $HF_{(g)}$ during the progressive addition of hot (915°C) magmatic gas into 1000 g of pure water initially at 25°C. Pressure was kept at 0.1 MPa throughout the simulation.

9). Changes in the concentration of dissolved HCl and HF with ξ are controlled by the dissociation reactions

$$HCl_{(aq)} = H^+ + Cl^- \quad (3.3)$$

and

$$HF_{(aq)} = H^+ + F^- \quad (3.4)$$

whose *pK* values at 100°C are –0.62 and 3.85, respectively. These *pK* values correspond to the iso-activity *pH*'s, where the activity of $HX_{(aq)}$ equals that of X^-. Since *pH* decreases regularly with ξ, the iso-activity condition is attained much earlier for HF than for HCl. The distribution of HF and F^- is further complicated by HF dimerization

$$2HF = H_2F_2 \quad (3.5)$$

and acid dissociation of the dimer

$$H_2F_2 = HF_2^- + H^+. \quad (3.6)$$

The evolution of dissolved S species (fig. 8) is rather complicated due to the occurrence of several association/dissociation and redox reactions (Symonds *et al*., 2001). Dissolved hydrogen sulfide is the dominant aqueous S species for $\xi \leq 3$ moles, whereas HSO_4^- ion prevails above this threshold, indicating an increase in f_{O_2}. Concurrently, the concentration of aqueous SO_2 increases, although it remains a subordinate S species throughout the process. Similar to what was observed for *pH* and Cl species, also some S species (*e.g*., HSO_4^- and SO_4^{2-}) experience dramatic changes approaching dry-up of the system.

3.5. *Chemistry of the gas phase*

In the biphase liquid-plus-gas region, the weight percentage of gases in the system considered increases almost linearly with ξ in the log-log plot of fig. 10, attaining 100% (dry-up of the system) for ξ of 79.3 moles. The gas phase is initially dominated by $CO_{2(g)}$, but $H_2O_{(g)}$ becomes the prevailing gas species for $\xi \geq 4$ moles (fig. 11). Hydrogen sulfide is the third major gas species through most of the biphase liquid-plus-gas region. Approaching dry-up of the system, $HF_{(g)}$ first and $HCl_{(g)}$ and $SO_{2(g)}$ afterwards appear in the gas phase and their concentrations increase progressively with ξ. In particular, $HCl_{(g)}$ experiences a large increase soon before dry-up and becomes the third major gas species, due to the high concentration of $HCl_{(aq)}$ in the «last drop» of liquid.

In the single gas region, $H_2O_{(g)}$ and $CO_{2(g)}$ are the two main constituents, initially followed by $HCl_{(g)}$, whose molar fraction decreases with ξ. On the contrary, the concentrations of $SO_{2(g)}$, $H_{2(g)}$, $S_{2(g)}$, and $CO_{(g)}$ increase by several orders of magnitude, and $H_{2(g)}$ becomes more important than $HCl_{(g)}$ for $\xi > 1600$ mol. Gas phases relatively rich in the magmatic component are characterised by similar concentrations of $SO_{2(g)}$, $H_2S_{(g)}$, $H_{2(g)}$, and $HCl_{(g)}$, whereas $CO_{(g)}$, $S_{2(g)}$, and $HF_{(g)}$ are present in lower amounts.

As already recalled, the similarity in $H_2S_{(g)}$ and $SO_{2(g)}$ molar fractions explains why redox conditions are consistent with the H_2S-SO_2 magmatic redox buffer of Giggenbach (1987).

4. Conclusions

The EQ3/6 software package, version 7.2, can be effectively used to compute the irreversible gas-water mass exchanges taking place during addition of magmatic gas to pure water at 0.1 MPa, in the liquid and liquid-plus-gas regions, similar to what was done by Symonds *et al*. (2001) by means of the software code CHILLER. However some post-calculations are needed to take in due account the effects of gas separation. In this specific case, these post-calculations were simplified by concurrent precipitation of crystalline α-sulfur, which fixes the redox potential. Post-calculations might be not as simple as in this case if precipitation of elemental sulfur does not take place. Luckily, this process is ubiquitous and precocious, considering that it begins upon addition of 0.45 g of magmatic gas only, at least in the case considered.

Since reaction path modeling is largely based on the assumption of conservation of enthalpy upon water-gas mixing, we reviewed the

enthalpies of the gas species of interest, adopting as reference state the liquid phase at the triple point. Used data are presented (table II) for comparison with other possible test cases.

Our results of geochemical modeling are very similar to those obtained by Symonds *et al*. (2001), apart from minor differences due to our choice of modeling magmatic gas scrubbing by pure water rather than by air-saturated water, as done by Symonds *et al*. (2001).

As already shown by Symonds *et al*. (2001), results of reaction path modeling carried out in this investigation indicate that scrubbing by water prevents significant emissions of strongly acidic gas species ($SO_{2(g)}$, $HCl_{(g)}$, and $HF_{(g)}$) until dry conditions are established, at least locally. However substantial $HCl_{(g)}$ degassing can occur from acidic brines rich in $HCl_{(aq)}$. These results are also consistent with the rule of thumb which is generally used to distinguish SO_2-, HCl-, and HF-bearing magmatic gases from SO_2-, HCl-, and HF-free hydrothermal gases (Giggenbach, 1980, 1987; Chiodini *et al*., 1993).

Finally, we would like to emphasize once more the power of reaction path modeling, which is also highly recommended for the correct interpretation of isotope data, especially multivalent elements, *e.g*., sulfur (*e.g*., Gambardella, 2001; Marini *et al*., 2002).

Acknowledgements

We thank Roberto Moretti, Paolo Papale, and Guido Ventura for the excellent organisation of the ESF LESC Exploratory Workshop «Gases in magmatic evolution: from depth to atmosphere, from micro to macro-scale, from calculation to observation», held in Rome on 11-13 May 2003.

We express our appreciation to Giovanni Chiodini, Johan Varekamp, and Ünsal Gemici for their constructive comments on the first version of the manuscript.

Our contribution was inspired by the outstanding 2001 paper by Robert Symonds, Terrence Gerlach, and Mark Reed, who really did a great job. We do not intend to rival with them but to pay a tribute to them, stressing once more the importance of geochemical modeling to understand natural processes.

REFERENCES

Benson, S.W. (1968): *Thermochemical Kinetics* (Wiley, New York), pp. 223.

Castellan, G.W. (1971): *Physical Chemistry* (Addison Wesley, Reading, Massachusetts), 2nd edition, pp. 866.

Chase, M.W. Jr. (1998): NIST-JANAF Thermochemical tables, *J. Phys. Chem. Ref. Data*, *Monogr. No. 9*, 4th edition, pp. 1951.

Chiodini, G., R. Cioni and L. Marini (1993): Reactions governing the chemistry of crater fumaroles from Vulcano Island, Italy, and implications for volcanic surveillance, *Appl. Geochem*., **8**, 357-371.

Chiodini, G., R. Avino, S. Caliro, D. Granieri, C. Minopoli, R. Moretti, L. Perrotta and M. Russo (2002): Relazione sulle emissioni gassose antistanti l'Isola di Panarea (novembre-dicembre 2002), *OV-INGV Rep*., pp. 13.

Delmelle, P. and A. Bernard (2000): Volcanic lakes, in *Encyclopedia of Volcanoes*, edited by H. Sigurdsson, B.F. Houghton, S.R. McNutt, H. Rymer and J. Stix (Academic Press, San Diego), 877-895.

Denbigh, K. (1971): *The Principles of Chemical Equilibrium* (Cambridge University Press), 3rd edition, pp. 494.

Gambardella, B. (2001): Concentrazione e rapporto isotopico dello zolfo dei fluidi fumarolici della Solfatara di Pozzuoli e di altre manifestazioni campane, *OV-INGV Rep*. (unpublished).

Giggenbach, W.F. (1980): Geothermal gas equilibria, *Geochim. Cosmochim. Acta*, **44**, 2021-2032.

Giggenbach, W.F. (1987): Redox processes governing the chemistry of fumarolic gas discharges from White Island, New Zeland, *Appl. Geochem*., **2**, 143-161.

Giggenbach, W.F. (1997): The origin and evolution of fluids in magmatic-hydrothermal systems, in *Geochemistry of Hydrothermal Ore Deposits*, edited by H.L. Barnes (John Wiley & Sons, New York), 3rd edition, 737-796.

Helgeson, H.C. (1968): Evaluation of irreversible reactions in geochemical processes involving minerals and aqueous solutions, I. Thermodynamic relations, *Geochim. Cosmochim. Acta*, **32**, 853-877.

Helgeson, H.C. (1969): Thermodynamics of hydrothermal systems at elevated temperatures and pressures, *Am. J. Sci*., **267**, 729-804.

Helgeson, H.C. and D.H. Kirkham (1974): Theoretical prediction of the thermodynamic behavior of aqueous electrolytes at high pressures and temperatures, I. Summary of the thermodynamic/electrostatic properties of the solvent, *Am. J. Sci*., **274**, 1089-1198.

Helgeson, H.C., R.M. Garrels and F.T. Mackenzie (1969): Evaluation of irreversible reactions in geochemical processes involving minerals aqueous solutions, II. Applications, *Geochim. Cosmochim. Acta*, **33**, 455-481.

Johnson, J.W., E.H. Oelkers and H.C. Helgeson (1992): supcrt92: a software package for calculating the standard molal thermodynamic properties of minerals, gases, aqueous species, and reactions from 1 to 5000 bar and 0 to 1000°C, *Comput. Geosci*., **18**, 899-947.

Keenan, J.H., F.G. Keyes, P.G. Hill and J.G. Moore (1978): *Steam Tables. Thermodynamic Properties of Water Including Vapor, Liquid, and Solid Phases (In-*

ternational System of Units – SI), (Wiley, New York), pp. 162.

LE GUERN, F., T.M. GERLACH and A. NOHL (1982): Field gas chromatograph analyses of gases from a glowing dome at Merapi volcano, Java, Indonesia, 1977, 1978, 1979, *J. Volcanol. Geotherm. Res.*, **47**, 223-245.

LIDE, D.R. (2002): *CRC Handbook of Chemistry and Physics* (CRC Press, Boca Raton), pp. 2664.

MARINI, L., B. GAMBARDELLA, C. PRINCIPE, A. ARIAS, T. BROMBACH and J.C. HUNZIKER (2002): Characterization of magmatic sulfur in the Aegean Island Arc by means of the $d^{34}S$ values of fumarolic gases, elemental sulfur, and hydrothermal gypsum of Nisyros and Milos islands, *Earth Planet. Sci. Lett.*, **200**, 15-31.

MARINI, L., A. YOCK FUNG and E. SANCHEZ (2003a): Use of reaction path modeling to identify the processes governing the generation of neutral Na-Cl and acidic Na-Cl-SO_4 deep geothermal liquids at Miravalles geothermal system, Costa Rica, *J. Volcanol. Geotherm. Res.*, **128**, 363-387.

MARINI, L., M. VETUSCHI ZUCCOLINI and G. SALDI (2003b): The bimodal *pH* distribution in volcanic lake waters, *J. Volcanol. Geotherm. Res.*, **121**, 83-98.

REED, M.H. (1997): Hydrothermal alteration and its relationship to ore fluid composition, in *Geochemistry of Hydrothermal Ore Deposits*, edited by H.L. BARNES (John Wiley & Sons, New York), 3rd edition, 303-366.

ROWE, G.L. JR., S. OHSAWA, B. TAKANO, S.L. BRANTLEY, J.F. FERNANDEZ and J. BARQUERO (1992): Using crater lake chemistry to predict volcanic activity at Poás volcano, Costa Rica, *Bull. Volcanol.*, **54**, 494-503.

SYMONDS, R.B., W.I. ROSE, G.J.S. BLUTH and T.M. GERLACH (1994): Volcanic-gas studies: methods, results, and applications, in *Volatiles in Magmas*, edited by M.R. CARROLL and J.R. HOLLOWAY, *Rev. Mineral.*, **30**, 1-66.

SYMONDS, R.B., T.M. GERLACH and M.H. REED (2001): Magmatic gas scrubbing: implications for volcano monitoring, *J. Volcanol. Geotherm. Res.*, **108**, 303-341.

VAREKAMP, J.C., G.B. PASTERNACK and G.L. JR. ROWE (2000): Volcanic lake systematics, II. Chemical constraints, in *Crater Lakes*, edited by J.C. VAREKAMP and G.L. ROWE JR., *J. Volcanol. Geotherm. Res.*, **97**, 161-179.

VAREKAMP, J.C., A.P. OUIMETTE, S.W. HERMAN, A. BERMÚDEZ and D. DELPINO (2001): Hydrothermal element fluxes from Copahue, Argentina: a «beehive» volcano in turmoil, *Geology*, **29**, 1059-1062.

WOLERY, T.J. (1992): EQ3NR, a computer program for geochemical aqueous speciation-solubility calculations: theoretical manual, user's guide and related documentation (version 7.0), *Rep. UCRL-MA-110662 PT III* (Lawrence Livermore National Laboratory, Livermore).

WOLERY, T.J. and S.A. DAVELER (1992): EQ6, a computer program for reaction path modeling of aqueous geochemical systems: theoretical manual, user's guide, and related documentation (version 7.0), *Rep. UCRL-MA-110662 PT IV* (Lawrence Livermore National Laboratory, Livermore).